Silicon (2020) 12:2165–2178
https://doi.org/10.1007/s12633-019-00307-1

ORIGINAL PAPER

Thermodynamic Phase Diagram, Half-Metallic and Optical Properties of the Zr_2TiSi [111] Films Based on DFT

Nosrat-Ali Vahabzadeh[1] · Arash Boochani[2] · Seyed Mohammad Elahi[3] · Hossein Akbari[1]

Received: 11 July 2019 / Accepted: 25 October 2019 / Published online: 4 January 2020
© Springer Nature B.V. 2020

Abstract

Thermodynamic stability, electronic and optical properties of the Zr_2TiSi compound in the bulk and its [111] films have been investigated, based on the density functional theory (DFT) framework and generalized gradient approximation (GGA). The Zr_2TiSi has thermodynamic phase diagram and mechanical stability in the bulk form. Also, the thermodynamic phase diagrams of the [111] films referred to good stability for three ZrSi-, ZrTi and SiZr-terminations. The Zr_2TiSi has ionic bonds between its atoms with brittleness behaviour. These films have half-metallic behaviour with $4.22\mu_B$, 4.33 μ_B and $8.61\mu_B$ magnetic moments for the ZrSi, ZrTi- and SiTi-terminations, respectively. Also, the optical property of the films have confirmed its metallic behaviour and its main optical response occurred in the infrared and visible ranges with the redshift than bulk one. The very low Eloss in the infrared (IR), visible and ultraviolet (UV) edge with high absorption in these regions of the [111] terminations, make them as suitable cases for optoelectronic applications.

Keywords DFT · Zr_2TiSi [111] films · Thermodynamic phase diagram · Half-metal · Optic

1 Introduction

In the last years, investigation on Heusler compounds increased due to their different physical properties such as Half-metallic, magnetic shape memory effect, thermoelectric properties [1–6]. Therefore, the Heusler compounds have been attractive for spin electron injection [7], Giant and Tunnel magnetoresistance (GMR and TMR) [8], magnetic switching [9–13], magnetic memories [14]. Mostly, the small energy gap in minority spin, and being sensitive to the external magnetic field, make them suitable compounds for thermoelectric spin switch [15]. The Heusler compounds are divided into two main categories, full-Heuslers and half-Heuslers with XYZ and X_2YZ stoichiometry, respectively. While the X and Y belong to the transition metals, the Z is belonging to the III-V column of the periodic table [16].

✉ Arash Boochani
arash_bch@yahoo.com

[1] Department of Physics, Ardabil Branch, Islamic Azad University, Ardabil, Iran

[2] Department of Physics, Kermanshah Branch, Islamic Azad University, Kermanshah, Iran

[3] Department of Physics, Faculty of Sciences, Science and Research Branch, Islamic Azad University, Tehran, Iran

The high active metallic natures of the Zr and Ti elements with their lightweight, stiffness and lower oxidations have made them attractive cases in the alloy crystallization [17–19]. The Zr and Ti atoms have a lot of interest in creating the chemical bonds with Si atom. Accordingly, they have created different alloys of these three elements such as: Ti_3Si, ZrSi, $ZrSi_2$ and Zr_2Si in the bulk, film and two-dimension forms [20–23]. Recently, the Zr_2TiAl compound was synthesized [24] in the Heusler structure with X_2YZ stoichiometry by L21 space group which X atoms are in the (1/4, 1/4, 1/4) and (3/4, 3/4, 3/4), Y and Z located at (1/2, 1/2, 1/2) and (0, 0, 0) positions, respectively [25]. Also, the new Zr bases of the Heusleres investigated, theoretically and experimentally [24, 26–30]. Mostly, the Heusler compounds have ferromagnetic behaviour [29], and some others have semiconducting properties [30]. Mostly, these materials use in the film and interface forms in industry applications [31–33], which the surface effects are changed their physical properties.

The electronic and optical conductivity and high optical absorption in the metallic materials are interesting for optoelectronic and infrared sensor applications [34]. For increasing or changing the abovementioned properties in the materials, it can be considered the surface effects in the film structures.

Heusler compounds are often used as thin films in the electronics industry, and they grow on semiconductor substrates along the two [001] and [111] directions, mostly [35–38].

Because of their compatibility with the semiconductor crystal lattice, they use as a source of electron injection [39–46]. Given that the Zr_2TiSi compound becomes crystalline at the base of the F.C.C lattice and its thin film along the [111] direction has a hexagonal cross-section and corresponds to semiconductor substrates, so we investigated the half-metallic, stability and optical properties of the ZrSi-, ZrTi- and SiZr-terminations for [111] films. We expected that the surfaces effects in the films would significantly alter the electronic, thermodynamic stability and optical behaviour.

2 Computational Methods

The mechanical, electronic and optical properties and thermodynamic phase diagram of the Zr_2TiSi bulk and [111] films have been calculated based on density functional theory (DFT) framework by full potential linear augmented plane wave (FP-LAPW) with Wien2K code [47, 48]. The Kohn-Sham equations have calculated under the generalized gradient approximation (GGA) [49]. The muffin tin radii for all atoms selected to 2 (Bohr) and the separation energy between the core and valance levels was determined to −6 Reyd. The optimized input parameters such as RKmax, KPoint and lmax were selected to 8.5, (3000 for bulk, 400 for films) and 10, respectively. The convergence calculations are based on the electron charge to 0.000, and the atomic forces in the film structures are relaxed to 0.1 a.u./Reyd by mini-position command.

3 Bulk Properties

3.1 Structural Properties

To find the accurate results, in the first step, it must obtain the ground state point with its equilibrium volume. The total change energy of Zr_2TiSi versus its unit cell volume (E-V) and fit with the Brich-Murnaghan equation diagram is shown in Fig. 1(a) in the ferromagnetic (FM) and non-magnetic (NM) phases. It is shown that the minimum point in the E-V diagram of the FM phase is lower than the other one, which refers to its stability in the magnetic state. The E-V arc is indicated the Zr_2TiSi hardness with the bulk module of 116.64(GPa) (Table 1). Under the hydrostatic pressure (in the smaller volumes) the NM and FM phases graphs are tangent to each other and in the larger volumes the ferromagnetic (FM) one is completely stable than NM. The transition pressure of FM to NM in the smaller volumes calculated to 68.24 (GPa).

For a more detailed check on the stability of this compound, we have plotted the phonon dispersion diagram in Fig. 1(b). It clear that all phonon branches have positive sign that refers to its dynamic stability. The levels slopes around the Γ point have been shown functional heat capacity for this compound. Two frequency gaps have appeared in the 150 cm^{-1} to 160 cm^{-1} and 205 cm^{-1} to 235 cm^{-1} ranges, the absorption of infrared light does not occur in these frequencies ranges.

The stability of the bulk phase can be supported by the aid of the thermodynamic phase diagram as a useful tool for evaluating the stability of the compositions [50, 51]. Regarding the metallic nature and thus the higher tendency of the Zr and Ti atoms for bonding, their chemical potentials have been selected as the main variables for calculating the Gibbs free energy:

$$g^{Bulk}_{Zr_2TiSi}=2\mu_{Zr}+\mu_{Ti}+\mu_{Si} \quad (1)$$

The amounts of the chemical potentials have been adopted from the Wien2K outputs, and each one is restricted to a minimum and maximum thresholds beyond which the related atoms are totally absent or perfectly present. Therefore, accessible region among the permitted values of all chemical potentials expects as a condition for crystallization. Figure 2 confirms that such an accessible region which highlighted is allowed and thus the bulk Zr_2TiSi could be thermodynamically crystallized.

In the following, the elastic constants and related parameters such as hardness, bulk and shear moduli, brittleness and ductility of the Zr_2TiSi bulk have been investigated which contain helpful information about microscopic nature of this matter [52, 53]. The ductility or brittleness nature of the materials check by the bulk modulus to the shear modulus ratio (B/G) which are ductile if the B/G be higher than 1.75 and brittle if be less than 1.75 amount [54]. The type of atomic bonds checks with the Cauchy pressure $(C_{12}-C_{44})$ that is positive for ionic bonds and negative for covalent ones [55]. The Poisson's ratio is another tool to compute the bond nature that for ionic (covalent) bonds is higher (less) than 0.25. The resistance of the materials to an applied force which named stiffness includes essential information about mechanical properties. High Young's moduli or elastic constants refer to the stiff material, and the flexible materials have low stiffness. The resistance to localized plastic deformations (shape changes) known as hardness which defined as bulk modulus, shear modulus and Vicker's hardness. The average sound velocities (V_a), Debye temperature (T_D) and melting point (T_m) of the Zr_2TiSi have been calculated by Hill scheme. Our simulated elastic constants of the bulk Zr_2TiSi, as well as some other mechanical and thermodynamic factors, are summarized in Table 1. Quickly using the data, the Cauchy pressure is positive, and therefore this bulk structure is dominantly ionic. This deduction is affirmed by the negative sign of the Vicker's hardness and the magnitude values of the Poisson's. The Young's modulus and $\left(\frac{B_H}{G_H}\right)$ ratio is 116.05 GPa and 0.17, implying the ductile nature of the composition. The objective

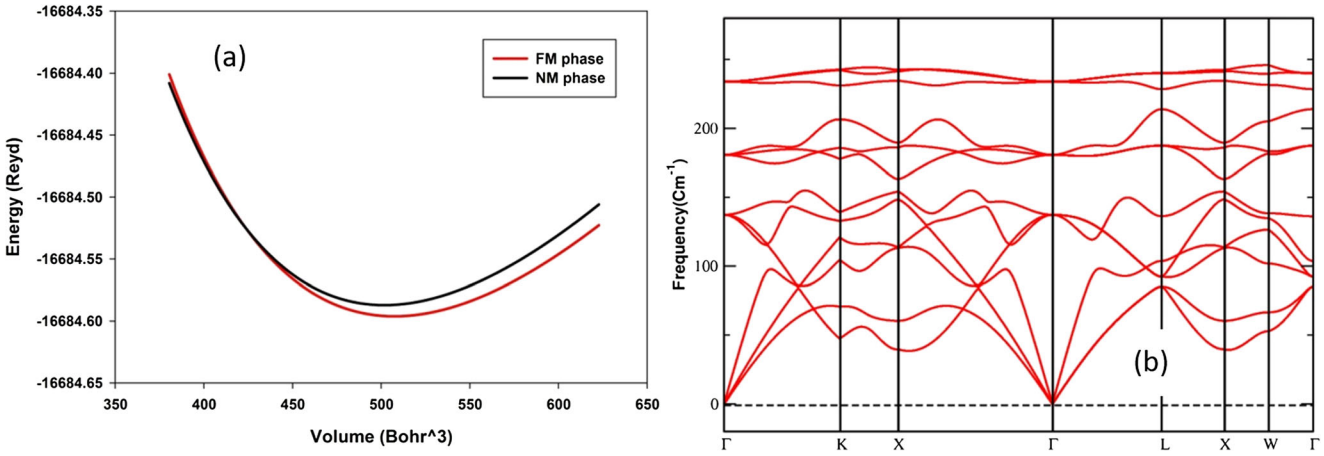

Fig. 1 **a** The energy-volume (E-V) diagram of the Zr_2TiSi in the two ferromagnetic (FM) and non-magnetic (NM) modes **b** The phonon branches of the mentioned case in the Brillouin zone

criteria for elastic stability (Born stability conditions) can be checked by eigenvalues of the elastic constants matrix (***C***), with keeping in mind that they all must be positive [56–59]. The stability of compounds leads to the following linear set of equations for cubic symmetries:

$$C_{11}-C_{12} > 0 \quad ; \quad C_{11} + 2C_{12} > 0 \quad ; \quad C_{44} > 0$$

Which referred to the elastic stability for the Zr_2TiSi bulk. Also, the significant amounts of the B and G modulus are indicated the ionic and anisotropy elastic response of the Zr_2TiSi to the external stresses or strains which are in agreement with a significant amount of the anisotropy (A). The electron density (ED) curves in the *x*-*y* and along with the main diameter panels in the two up and down spins are in agreement with the A amount. It indicated the ionic bonds between atoms with different behaviour along with the mentioned directions. The strong bonds between atoms are caused by high Debye and melting point temperatures (Table 1).

3.2 Electronic Properties

The density of states (DOS) and bandstructure of the bulk Zr_2TiSi in the two up and down spins have been depicted in Fig. 3. It is shown that this compound has the half-metallic nature with 65% spin polarization at Fermi level. The DOS curves are shown good metallic behaviour for two mentioned spins as the electron states are extended from valence band to the conduction one. Also, the bandstructures in the first Brillouin zone along the symmetry points are depicted in the Fig. 3 for two mentioned spins. The energy levels cut the Fermi surface in the two up and down spins, while in the down spin several levels have been cut off the Fermi level with different gradients and are convolve of valence to conduction bands which referred to its high metallic behaviour with good electron transports. Although the DOS curve shows the electron probability in the Fermi level in the up spin, but the level that cut the Fermi level (belong to Zr d orbital) is smooth, completely, which is referred to the zero velocity of its electrons and infinity effective mass, so its electrons no contribution in the electronic conductivity. Thus, the Zr_2TiSi in this spin mode behaves like a semiconductor. Also, the ED diagram indicated the ionic spin bonds that changed as the external magnetic field. In the *x*-*y* panel, the main ionic bonds are occurred between Ti atoms in the up spin and between the Ti and Si atoms in the down spin. In the main diameter of the unit cell, the ionic bonds are between the Ti and Zr atoms in up spin and are between the Zr and Ti with Si in down one Fig. 4.

The optical diagrams of the Zr_2TiSi bulk have been depicted in Fig. 5. The real part of the dielectric function (Epsilon-Re) indicates the metallic behaviour of this case in lower energies and has the infinite amount in the zero photon energy. This diagram is decreased by sleep slope as increasing the photon energy and entering to the negative area at the ultraviolet (UV) edge, and till 16.5 eV its response to the incident light is negative. The Epsilon-Re has two roots in the UV edge and 20 eV that can be originated from the plasmonic oscillations. It should be noted that the main optical responses have occurred in the infrared (IR) and visible areas. The imaginary part of dielectric function (Epsilon-Im) is the

Table 1 The lattice constant a(A°), elastic constants C_{ij}(GPa), Bulk module B(GPa), Shear module G(GPa), Yong module E(GPa),Poisson's coefficient ν, elastic anisotropy A, average wave velocity V_a, Debye temperature T_D (K) and melting point T_m (K).

A	C_{11}	C_{12}	C_{44}	B	G	E	ν	A	V_a	T_D	T_m
6.698	474.30	63.07	1185.64	116.05	660.09	683.79	−0.48	4.41	11,371.62	1273.12	3356.15

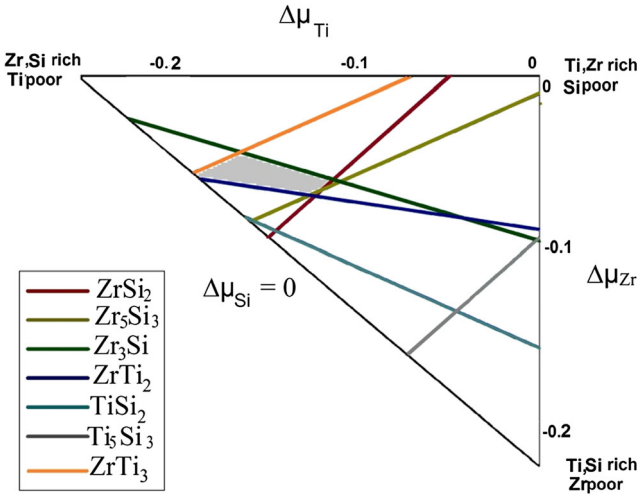

Fig. 2 The thermodynamic phase diagram of the Zr_2TiSi bulk as atomic, chemical potentials. (The accessible region is highlighted)

optical response of the matter to the light in the energy space so that each peak indicates the optical transition of the full level to the empty one. The Epsilon-Im agrees with the metallic nature of this compound, whereas its static amount is none zero and also, its main peak is laid in the IR region. By increasing the photon energy the Epsilon-Im diagram has dropped sharply and reached to zero after 10 eV photon energy which is indicated no electron transition after this energy. The energy loss function (Eloss) means losing photon energy in the matter. The Eloss diagram of the Fig. 5 has been shown no peak in the IR, visible and UV areas till 20 eV, by comparison between the Epsilon-Re and Eloss diagrams, it showed that the plasmonic oscillations occurred in the 20 eV. The important note to pay attention to is that the Eloss has any peak in the IR and visible areas, and also the main optical responses occur in these energy ranges, which referred to its photo sensor applications at these energies. Based on the metallic nature of Zr_2TiSi bulk in the IR and visible spectra, the

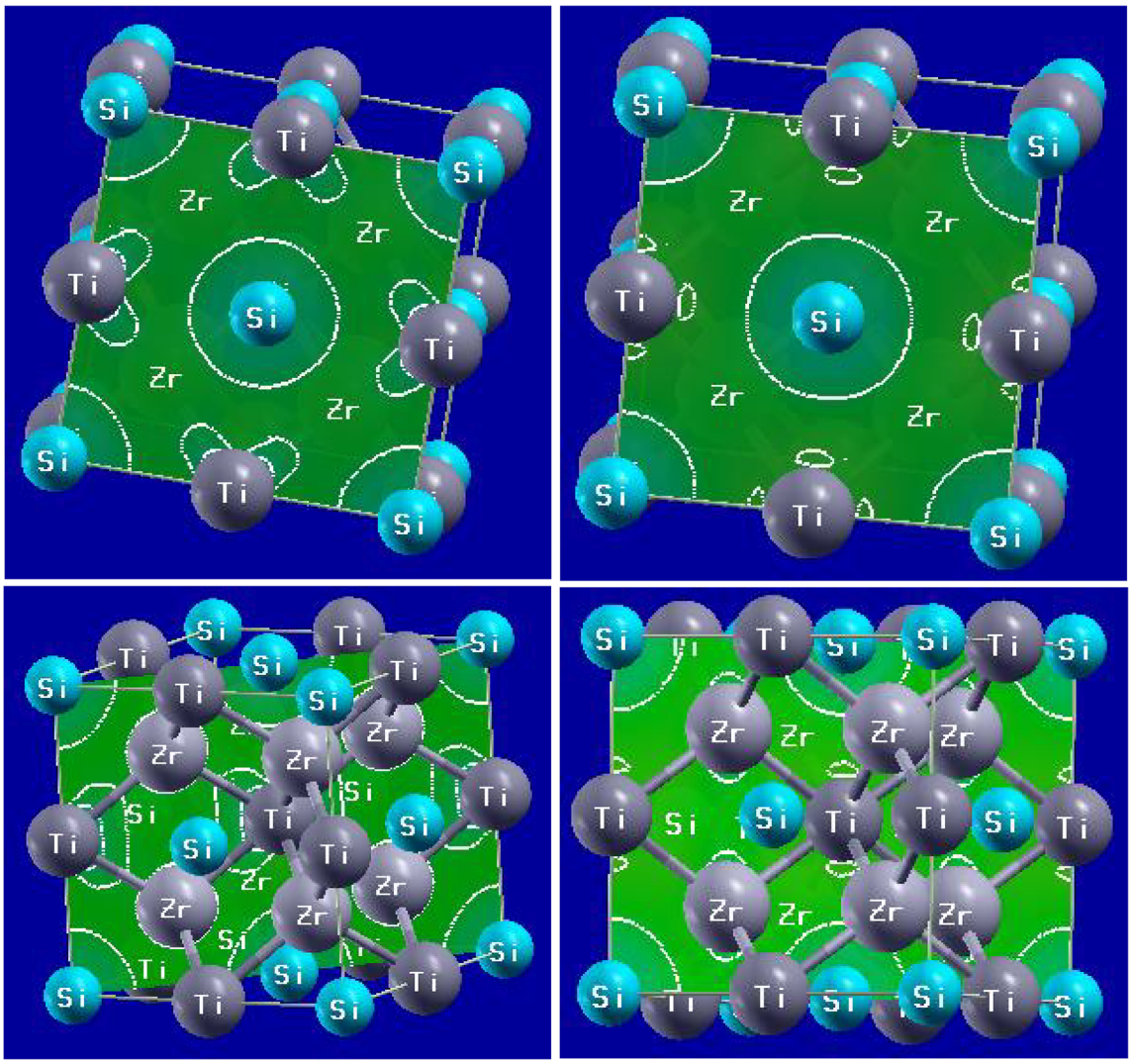

Fig. 3 The electron density (ED) in the x-y (top) and main diameter (down) planes for the two up (left column) down (right column)

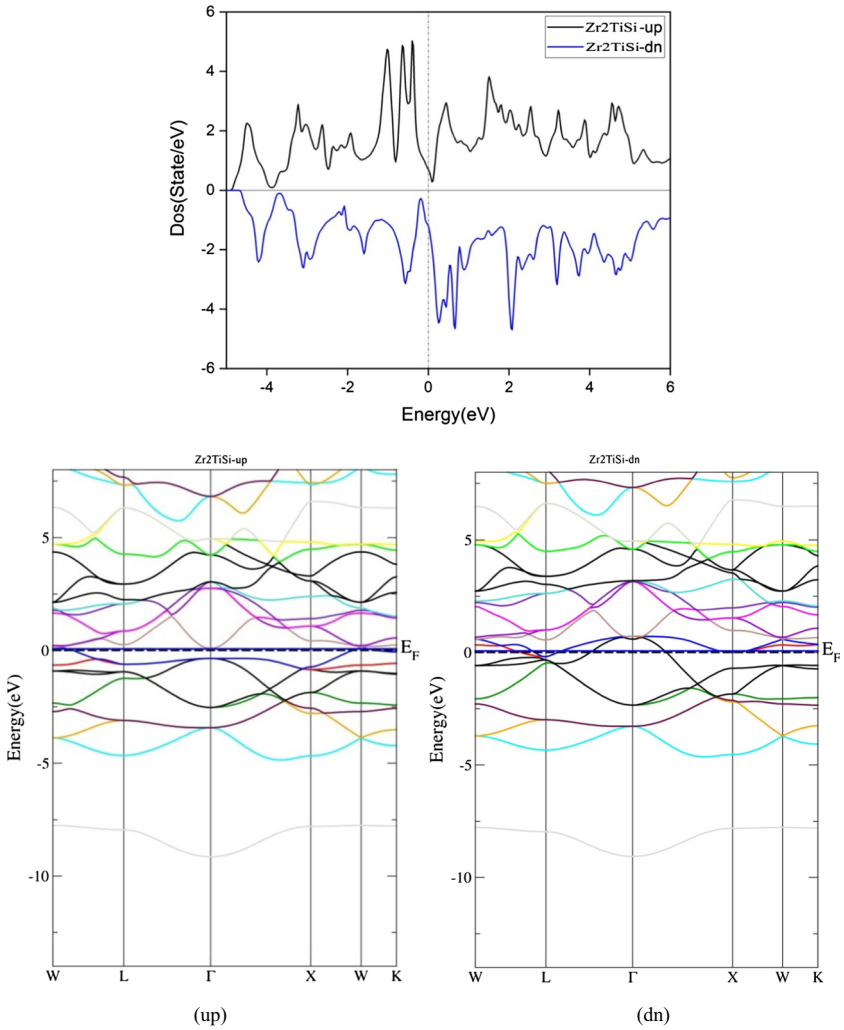

Fig. 4 The DOS (top) and band structure (down) in the up and down spins of the Zr_2TiSi bulk

main extinction peaks total change in these areas its curve decreased in the higher photon energies, so the light absorption is little in lower energies and at higher energies based on reducing the extinction and refraction indexes, this compound is same of the transparent matter. Also, the reflection index confirmed the metallic nature of the Zr_2TiSi bulk in lower energies and at higher energies behaves like a transparent object.

4 Film Properties

4.1 Electronic Properties

The surface effects in the film are the main reason for change electronic and optical behaviour. These changes are originated of the increasing the electron density (ED) in the surface layer and appearing the dangling bonds in this layer. The Zr_2TiSi films can be crystalized along with its symmetric directions of the unit cell such as [001], [010], [111] etc. The [111] film of the FCC crystals as Heusler compounds are the important case base the Hexagonal geometry cross-section. The [111] supercells of the Zr_2TiSi compound with various terminations are shown in Fig. 6, whereas their ED in the surface layers has been depicted in the two up and down spins. The ED of the three ZrTi-, ZrSi and SiZr-terminations are depicted in Fig. 6 in the two up and down spins. The surface ED of the film terminations indicated the ionic bonds between the surface atoms. The ED geometry in the down spin for the Zr atom shows the electronic polarization than other cases in the surfaces of the film in down spin which referred to the ionic property than up one. The ZrSi-, SiZr- and ZrTi-terminations have the magnetic moments of 4.22 μ_B, 4.33 μ_B and 8.61 μ_B, respectively, which indicated these films are suitable cases for the spintronic applications.

up dn up dn up dn.

The electron density of states (DOS) contains important information about the electronic and optical properties of the materials. The DOS diagrams of the abovementioned thin films have been depicted in the Fig. 7 in the two up and down spins. It is shown that all three terminations have the DOS anisotropy in the two up and down spins which refer to the

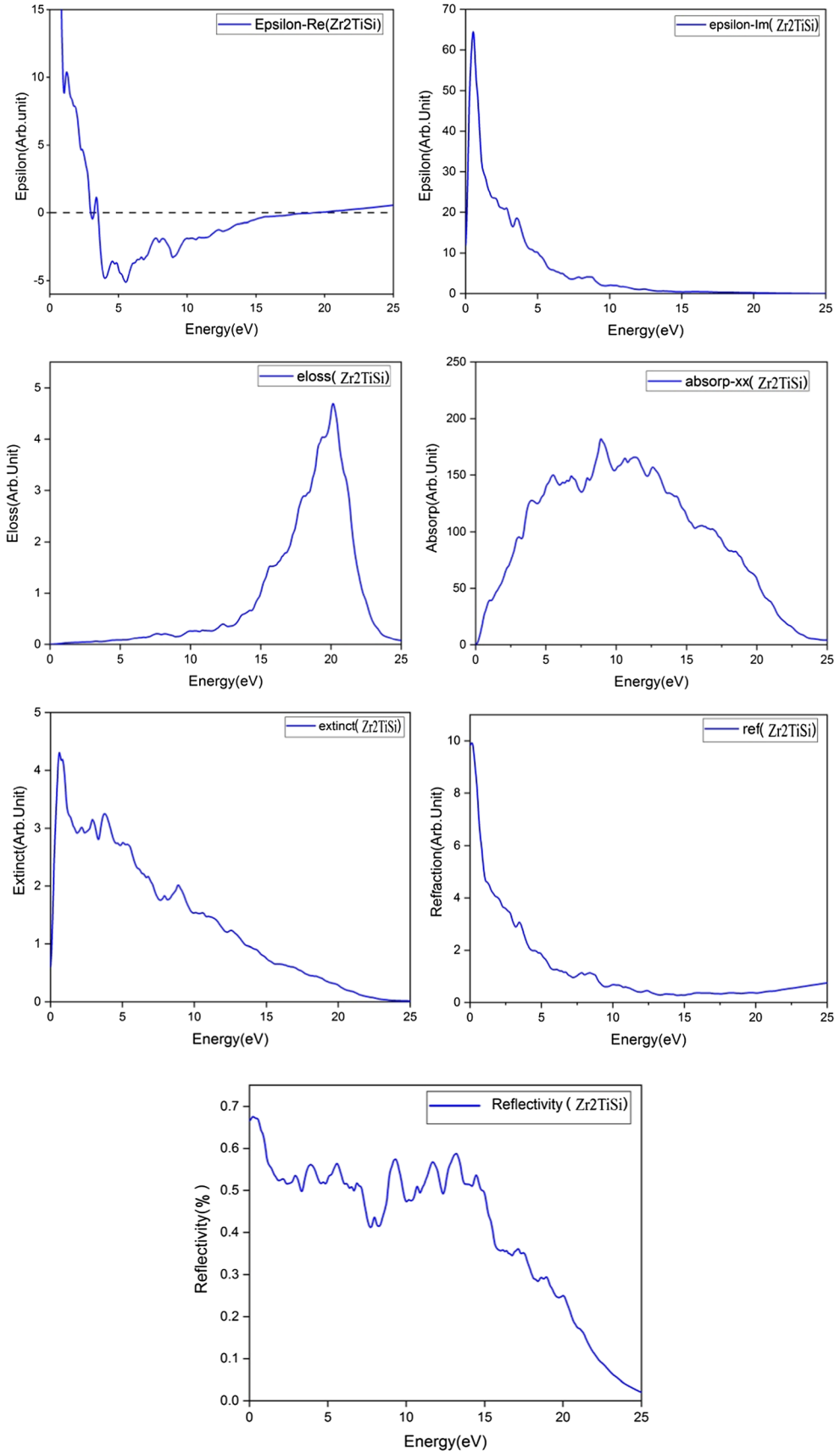
Epsilon-Re(Zr2TiSi)
Epsilon(Arb.unit)
Energy(eV)
epsilon-Im(Zr2TiSi)
Epsilon(Arb.Unit)
Energy(eV)
eloss(Zr2TiSi)
Eloss(Arb.Unit)
Energy(eV)
absorp-xx(Zr2TiSi)
Absorp(Arb.Unit)
Energy(eV)
extinct(Zr2TiSi)
Extinct(Arb.Unit)
Energy(eV)
ref(Zr2TiSi)
Refraction(Arb.Unit)
Energy(eV)
Reflectivity (Zr2TiSi)
Reflectivity(%)
Energy(eV)

◀ **Fig. 5** The real and imaginary parts of the dielectric function, Eloss, Absorption, Extinction, Refraction and Reflection of the Zr_2TiSi versus photon energy

magnetic and half-metallic nature of these compounds. The ZrSi-termination has low spin polarization at Fermi level, and two others have higher magnetic behaviours which are in agreement with the ED curves in the Fig. 6. In spin down the electron, states have been shifted to higher energies, especially for the SiZr-termination case. So, these [111] thin films have the half-metallic nature with excellent electronic conductivity in the two mentioned spins. It is shown that the electron states are broadened of valence to the conduction bonds, continuously.

The electron levels diagrams in the first Briliuon zone along its symmetry directions (bandstructure) of the three mentioned Zr_2TiSi [111] film terminations had been drowned in the Fig. 8 for two up and down spins. The ZrSi-termination bandstructure has the interesting behaviour, whereas, in spite of the electron states at the Fermi level in up spin (Fig. 7), the level splitting is appeared in up spin with the direct energy gap in the *X* to *M* direction. The main electron states of this spin belong to the flat level near the Fermi level that its electrons have zero group velocity with infinite effective mass which no contribution in the electronic and optical conductivity. But the valence and conduction bonds interconnectedness at the Fermi level with various gradient indicated high electron mobility in this spin. As we expected of the high metallic nature of the Zr and Ti atoms in the surface of the ZrTi-termination case, the bandstructure diagrams for this termination in the up and down spins have metallic behaviour by the high gradient of their levels. The presence of the Si atom in the film surface of the SiZr-termination case has been changed its electronic structure than last case. It is shown that the splitting of the levels is appeared in the Fermi level in the up spin, even though it has the electron states in its DOS diagram from Fig. 7. As the ZrSi-termination case, in the SiZr-termination exist a flat level upper the Fermi level. The group velocity in this level is zero, and also, the effective mass has infinite amount, so the SiZr-termination such as ZrSi- one has the semiconducting behaviour in the up spin. Also, the steep slope of the levels in all cases in the conduction bods indicated good electron mobility. Based on the narrow gap in the up spin of the ZrSi- and SiZr-termination cases and also, the levels density around the Fermi level these cases can be good thermoelectric properties.

4.2 Optical Properties

The optical properties of the Zr_2TiSi [111] films have calculated with random phase approximation (RPA) method based on Kramars-Kroing relations. The real and imaginary parts of the dielectric function coefficients are the main parameters for investigating the optical response of the matter to the incident light. Based on the symmetry of the mentioned films, we studied the two main directions, in-plane (*xx*) and perpendicular to it (*zz*). The real part of the dielectric functions (Epsilon-Re) has been painted along the *xx* and *zz* in the panels (a, b) in the Fig. 8. The static amounts of the Epsilon-Re are infinite for the two mentioned directions which referred to their metallic behavior. It is shown that the Epsilon-Re (*xx*) has a redshift than its amount in the *zz* direction. By increasing the photon energy, the Epsilon-Re is decreased until the ultraviolet (UV) edge in the two mentioned directions. Each Epsilon-Re of the two mentioned directions have two roots and have negative amounts of the UV edge to 13 eV photon energy. Comparing the Epsilon-Re of the bulk to the films indicate that the negative value of the films is decreased, so these [111] films have better optical responses to the incident light.

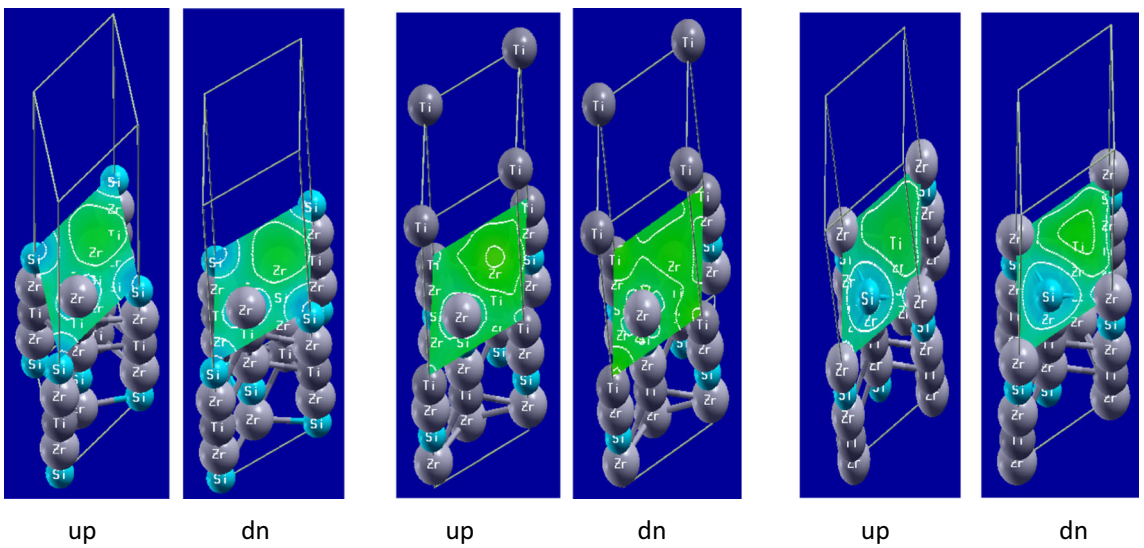

Fig. 6 The ZrSi-, ZrTi- and SiZr- terminations ED in the up and down spins (of left to right), respectively

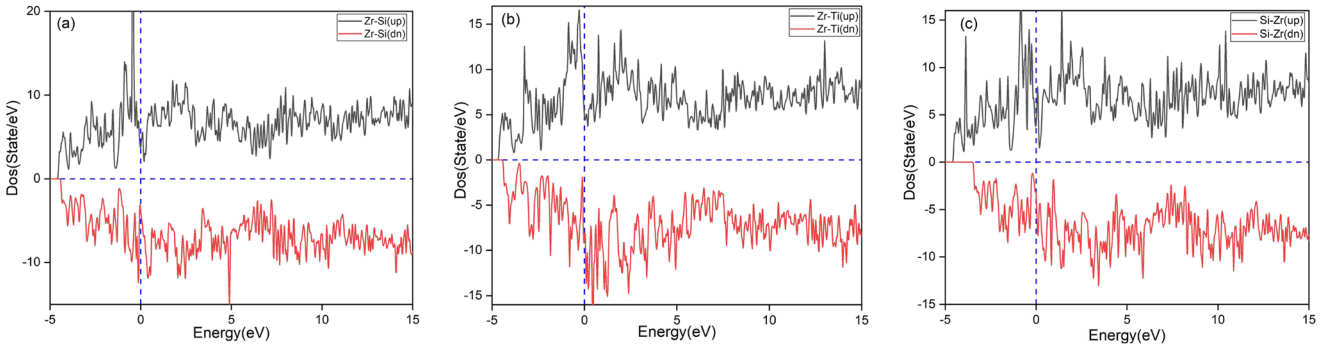

Fig. 7 The DOS diagrams of the **a** ZrSi-, **b** ZrTi- and **c** SiZr-terminations in the up and down spins

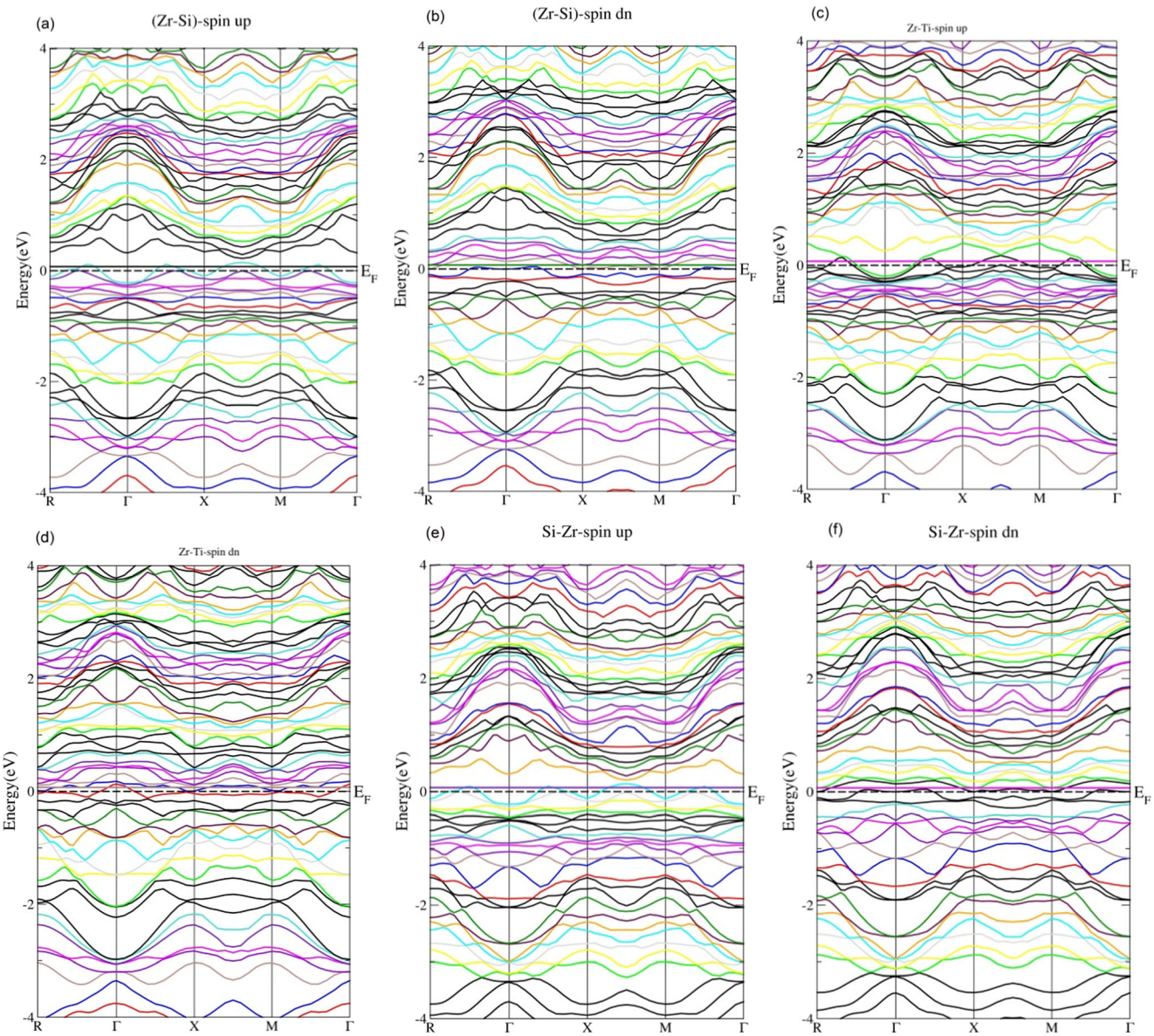

Fig. 8 The electronic bandstructure of the ZrSi-, ZrTi- and SiZr-terminations in the up and down spins

A negative Epsilon-Re sign means that light cannot pass through the material, and therefore the material does not give a reasonable response to the light. The concurrent negative values of Epsilon-Re and refraction indexes mean it refers to the meta-material nature. From the comparison of Figs. 9 and 11, we find that in the energy range that Epsilon-Re is negative, the refractions are shifted toward lower than one; therefore, these compounds have the potential to become meta-material in the 5 eV region.

The imaginary part of dielectric function (Epsilon-Im) has important information about electronic and optical properties. Each peak of the Epsilon-Im indicate the optical transitions of the excited electrons from the full level (under the Fermi level) of the Zr, Ti and Si atoms to empty ones, the Fig. 9(c, d) confirmed the metallic nature of these compound, especially along the *xx* direction. Along the *xx* direction, the optical transitions are occurred in the infrared (IR) to UV and have the redshift along the *zz* direction. For two mentioned directions no transitions occurred after 15 eV, which indicated no optical absorption in this area. Comparing the Epsilon-Im with Eloss, absorption and reflection diagrams have shown that after 15 eV photon energy, these compounds act as transparent materials.

The energy loss function (Eloss) diagram indicates losing of the optical energy of photons in the material. The Eloss curves of the Zr_2TiSi [111] films along the *xx* and *zz* directions have been depicted in the Fig. 10. It clear that these diagrams have their lowest amount in the IR and visible areas and the main peaks are occurred in the 13 eV photon energy, whereas the Epsilon-Re for these terminations is zero, which referred to the plasmonic oscillations. According to the small amounts of the Eloss in the lower energies, it can be said that these films are suitable cases for optical sensors in the IR and visible areas. On the other, it is clear that the absorptions for all cases have steep slopes in the lower energies and reach their saturation amounts in the UV edge to 10 eV. Based on the minimum amount of the absorption and Eloss after 20 eV and zero of the reflection, these cases behave as transparent materials.

The real and imaginary parts of the refraction index by names of extinction and refraction indexes are present in the Fig. 11 for the two *xx* and *zz* directions. It is shown

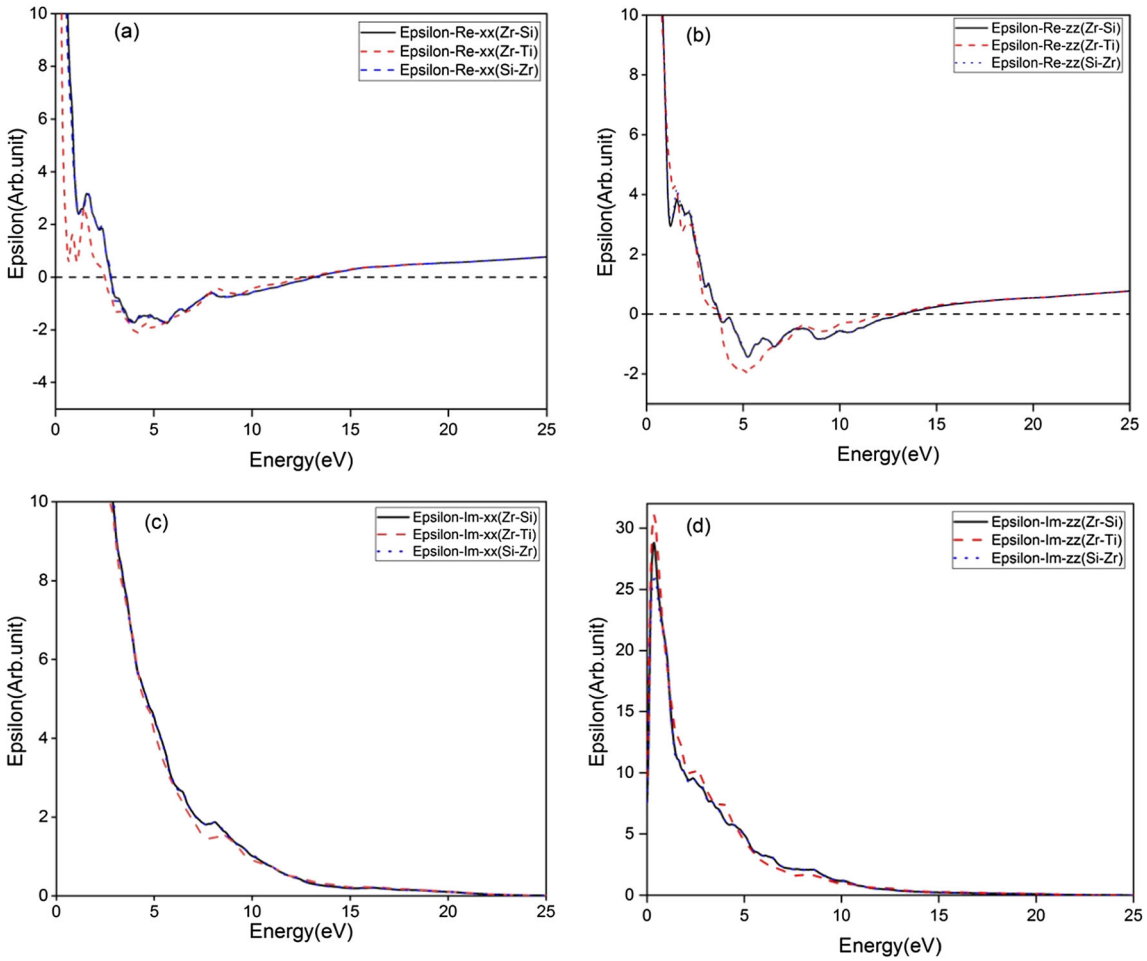

Fig. 9 The Epsilon-Re and Epsilon-Im of the ZrSi-, ZrTi- and SiZr-terminations along the *xx* and *zz* directions

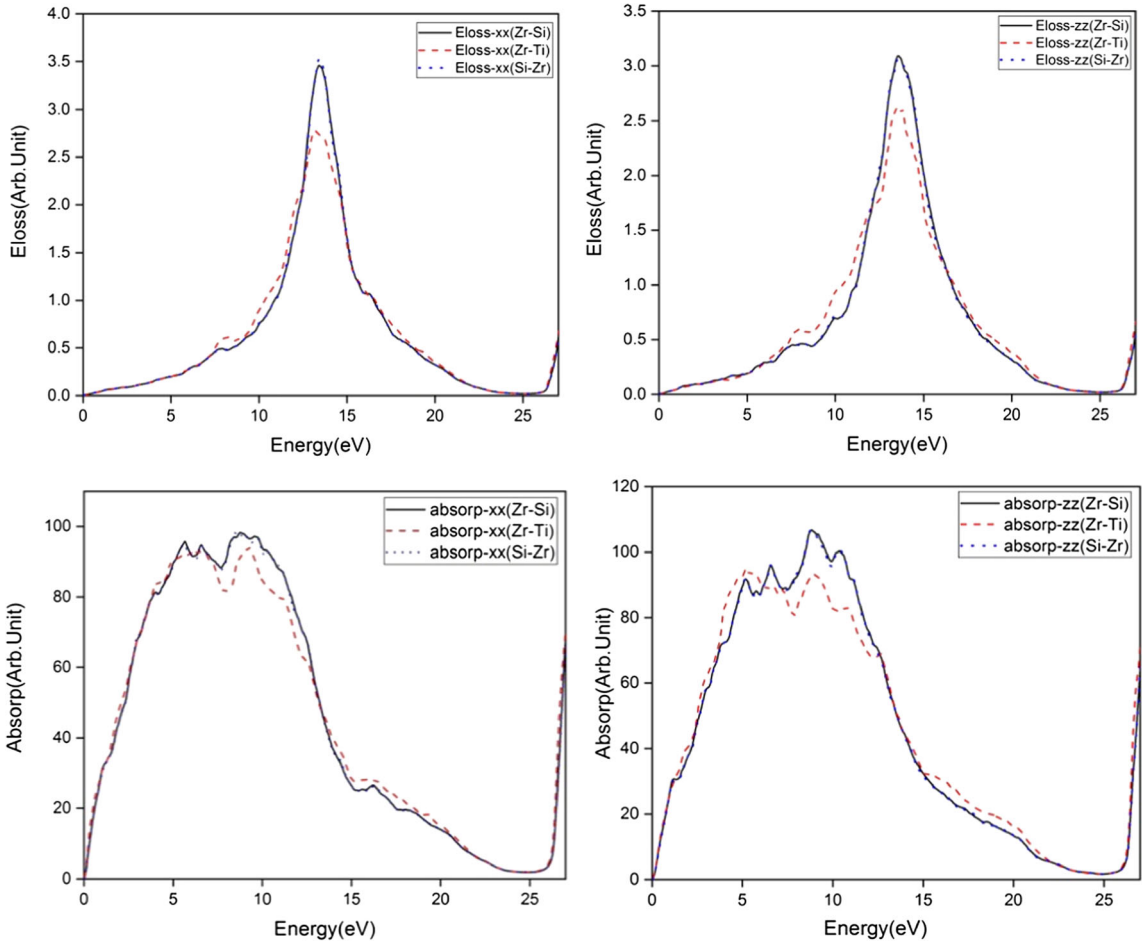

Fig. 10 The Eloss (top) and Absorption (down) diagrams of the ZrSi-, ZrTi- and SiZr-terminations along the two *xx* and *zz* directions.

that the maximum extinctions with drop electromagnetic wave amplitudes are occurred in near the zero energy, which is referred to the high metallic nature of these cases. By increasing the photon energy, the extinctions are decreased that indicated the transparent behaviour for these films along with two mentioned directions. But the extinction is started of zero for the *zz* direction cases. The refraction amounts along two mentioned directions in the IR have been indicated the metallic treatment. In the 5 eV photon energy, the refraction indexes are one, and this compound has similar to vacuum behaviour and after this energy, the refraction indexes have been shifted to lower than one which referred to higher electromagnetic speed than light.

The reflection indexes of the [111] films have depicted in the Fig. 12 for two *xx* and *zz* directions. It is shown that the amount of the static amount of reflections is 0.8 and 0.58 for the *xx* and *zz* directions, respectively, which referred to the high metallic nature for *xx* direction and lower for *zz* one in the IR region. But for all directions, after 15 eV, the reflection indexes are shifted to zero that are confirmed the transparent behaviours for these cases.

4.3 Thermodynamic Phase Diagram Properties

The thermodynamics can be a useful tool for studying the stability of different films, which is capable of examining the stability of different surfaces in real thermodynamic conditions. This theory assumes that each film is in equilibrium with the gas consisting of the constituent elements of that film. This gas environment acts as an endless source of particles at constant temperature and pressure. As we know, the stable atomic composition at each film depends on the ratio of the constituents of the gaseous environment. For example, if there is a higher percentage of Zr in the gaseous environment, then its concentration at the film will increase. To quantify the thermodynamic stability of surfaces, the free energy of the surfaces must be investigated that follow as bellow:

$$\gamma(T,P_i) = \left[G(T,P_i) - \sum_i N_I \mu_I(T,P_i)\right]/2A \qquad (2)$$

Which G is the Gibbs Free energy of the film, N_i and μ_i are the number of atoms in the film structure and chemical potential for each atoms, respectively. Also, T and P are the environment temperature and pressure, respectively. Hence, we calculated

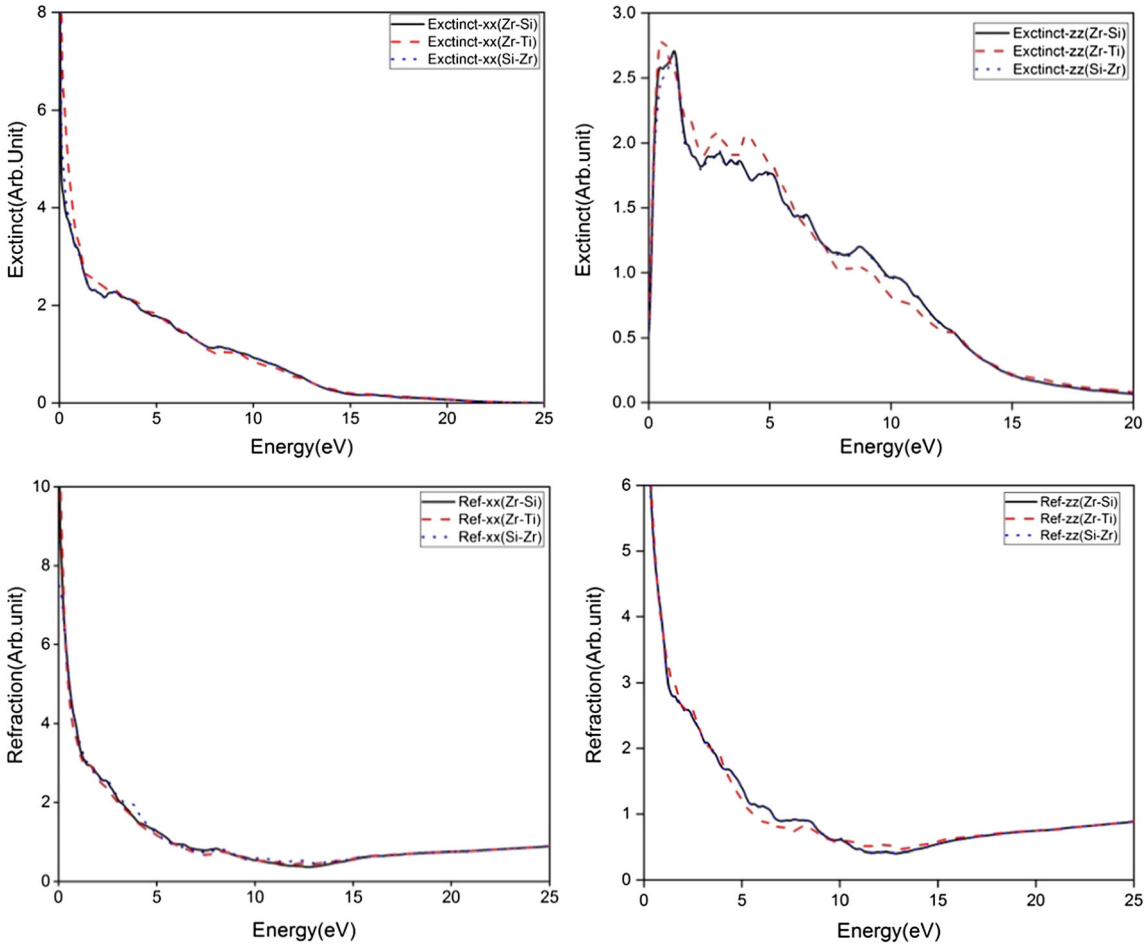

Fig. 11 The Extinction (top) and Refraction (down) indexes of the Zr_2TiSi [111] film for *xx* and *zz* directions.

the thermodynamic phase diagrams of the ZrSi, ZrTi and SiZr terminations of the Zr_2TiSi [111] films. In the stable film, the surface Gibbs energy must be in equilibrium with internal layers which have the bulk-like behaviour. In Fig. 13, the maximum value of the Zr and Ti chemical potentials are referred to their pure bulk phases and the minimum ones who obtained from Eq. 3, indicates conditions that the Zr (Ti) atoms leave the crystal structure. The Free energy of different films can be obtained in terms of different chemical potentials and phase diagrams can be drawn for all films. In the first step, we show the stability of the Zr_2TiSi compound in the full Heusler phase by calculating the total energy of the phase diagram. Gibbs free energy of this

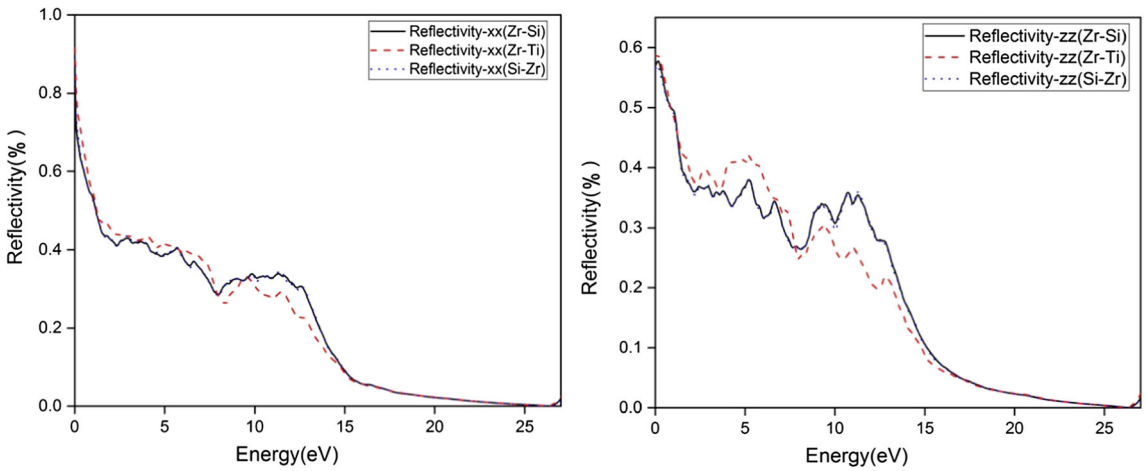

Fig. 12 The Reflection indexes of the [111] films along with the *xx* and *zz* directions

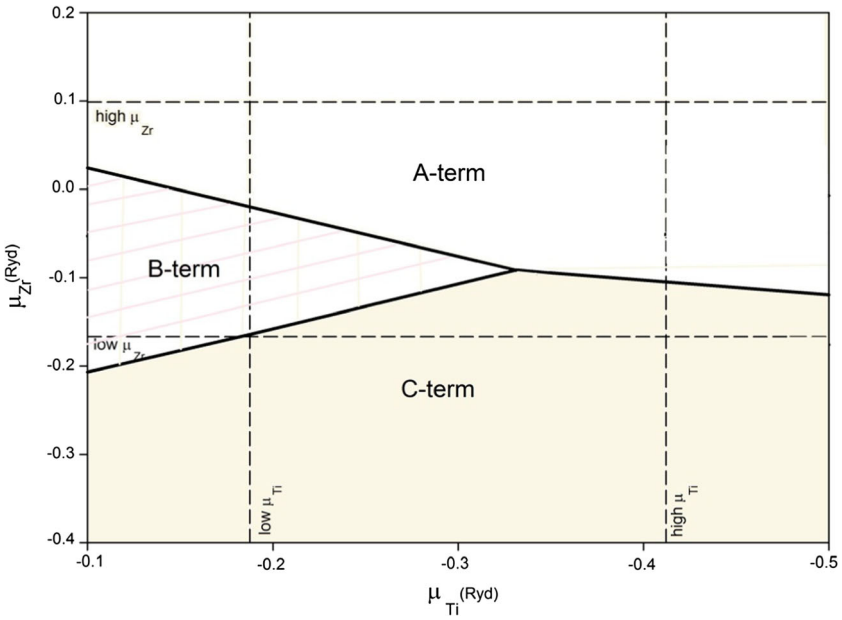

Fig. 13 The thermodynamic phase diagram of the ZrSi- (B-term), SiZr- (C-term) and ZrTi- (A-term) terminations based on the chemical potential of the Zr and Ti atoms

compound can be calculated according to the following equations in terms of the chemical potentials of the atoms forming it.

$$2\mu_{Zr} + \mu_{Ti} + \mu_{Si} = g^{bulk}_{Zr2TiSi} \tag{3}$$

Which μ_{Zr}, μ_{Ti} and μ_{Si} are chemical potentials of the Zr, Ti and Si, respectively, in the Zr2TiSi bulk.

To specify the accessible region, we use the following relationships:

$$1/2(G_{Zr2TiSi} - G_{TiSi}) \le \Delta\mu_{Zr} \le G^{bulk}_{Zr} \tag{4}$$

$$G_{Zr2TiSi} - G_{ZrTi} \le \Delta\mu_{Si} \le G^{bulk}_{Si} \tag{5}$$

$$G_{Zr2TiSi} - G_{ZrSi} \le \Delta\mu_{Ti} \le G^{bulk}_{Ti} \tag{6}$$

In the next step, we calculated the phase diagrams of the films, so the free energies can be obtained from the bellow relation.

$$\gamma_i(T, P_i) = \frac{\left(G^{slab} - \mu_{ZrN_{Zr}} - \mu_{TiN_{Ti}} - \mu_{SiN_{Si}}\right)}{2A} \tag{7}$$

That G^{slab} is the Gibbs free energy of the film, N_{Ti} N_{Si} and N_{Zr} are the atomic number in the film cell. The denominator 2 is referred to the two surfaces on both sides for each film structure. On the other hand, the films thickness are optimized that their middle layers exhibit bulk properties. Therefore, the surfaces can be considered in thermodynamic equilibrium with the bulk state, and according to the above eq. 2, the free surface energy can only be written in terms of the chemical potential of the two dominant atoms (ie, Zr and Ti):

$$\gamma_i(T, P_i) = \frac{\left(G^{slab} - \mu_{Zr\ \ (N_{Zr} - 2N_{Si})} - \mu_{Ti(N_{Ti} - N_{Si})}\right)}{2A} \tag{8}$$

The most important issue is the relation between Gibbs free energy and the results of our calculations in the context of density functional theory. Gibbs free energy consists of different parts:

$$G = E^{tot} + F^{vib} + PV \tag{9}$$

That E^{tot} is the total energy in ground state, F^{vib} is the portion of energy due to atomic vibrations, and PV has the small amount which can be ignored under the 100 atm pressure. To calculate the vibrational part, we need to use the phonon spectrum of the system, and if the density of the phonon states be the $\delta(\omega)$, the vibrational part of the Gibbs free energy is defined as follows:

$$F^{vib}(T, w) = \hbar w\left(\frac{1}{2} + \frac{1}{e^{\beta\hbar w} - 1}\right) - kT\left[\frac{\beta\hbar w}{e^{\beta\hbar w} - 1} - 1n\left(1 - e^{-\beta\hbar w}\right)\right] \tag{10}$$

But calculating the vibration part using the above method in our software is very time consuming. Because the computation of the phonon spectrum of thin-layers requires the use of large time and high computational volume. But one can ignore the share of vibrational energy with good accuracy. At stoichiometric surfaces (surfaces where the ratio of atoms is the same as the bulk),

Table 2 The Cohesive energy (E_C) and Enthalpy (H) of the ZrSi-, ZrTi- and SiZr-terminations versus eV

	ZrSi-terminations	ZrTi-terminations	SiZr-terminations
E_C	−5.35	−6.01	−5.41
H	−4.22	−4.81	−4.33

the free surface energy is $\gamma = (G^{slab} - Ng^{bulk})/2A$, which depends on the Gibbs energy difference between the surface and bulk states, and for non-stoichiometric levels, a similar argument can be applied. So we estimate the Gibbs free energy with the total energy calculated based on the density functional theory as the (8) relation.

Another problem here is that the energy of the super cell and bulk does not have a specific energy reference and their absolute value is meaningless. To measure these values from a physical reference point, we decided to measure the energy of each system relative to the energy of its atoms in isolation (because the chemical potential of the isolate atom is zero and can be a good energy reference point). In other words, we use the cohesive energy of that system instead of the total energy of each system. To complete the discussion of the stability of the film, we calculated the Cohesive energy (E_C) and Enthalpy (H) and our results are present in Table 2. It is shown that all terminations have stability in the abovementioned views based on their negative signs in the E_C and H parameters.

5 Conclusion

Thermodynamic phase diagram stability, elastic, electronic and optical properties of the Zr_2TiSi in bulk and its [111] films have been investigated by the DFT framework and GGA approximation. The EV diagrams indicated that the Zr_2TiSi has the ground state point in the ferromagnetic phase. Also, the phonon bandstructure indicated the dynamic stability of the Zr_2TiSi. The thermodynamic phase diagrams of the bulk and film cases referred to their stability as the thermodynamic view. The elastic constants results and relative parameters showed to the ionic bonds between atoms with brittleness behaviour and excellent elastic stability. The DOS and bandstructure curves have been shown the half-metallic nature of this compound with 65% spin polarization on the Fermi level. Also, the electron density on the slabs confirmed the magnetic property with ionic bonds between atoms.

It was observed that there were thermodynamic stability in all fims terminations, especially the ZrTi one. The surface effects have led to spin splitting of the ZrSi- and SiZr-terminations in the up spin, which gives rise to the half-metallic behavior. The ED diagrams of the films surfaces have confirmed the ionic bonds in the films surface.

The positive optical responses of films are occurred in the IR and visible regions and have the redsfift than bulk case. Also, very low amount of the energy loss function in the abovementioned energy ranges with high absorption and Epsilon-Im have indicated that these films can be suitable cases for opto-electronic applications.

References

1. Roy S, Khan N, Singha R, Pariari A, Mandal P (2019). Phys Rev B 99:214414
2. Guillemard C, Petit-Watelot S, Pasquier L, Pierre D, Ghanbaja J, Rojas-Sánchez J-C, Bataille A, Rault J, Le Fèvre P, Bertran F, Andrieu S (2019). Phys Rev Appl 11:064009
3. Lidig C, Minár J, Braun J, Ebert H, Gloskovskii A, Krieger JA, Strocov V, Kläui M, Jourdan M (2019). Phys Rev B 99:174432
4. Yamada S, Kobayashi S, Kuroda F, Kudo K, Abo S, Fukushima T, Oguchi T, Hamaya Phys K (2018). Rev Materials 2:124403
5. Nehra J, Jani S, Dolia SN, Lakshmi N (2019). J Magn Magn Mater 481:6
6. Idrissi S et al (2019). Phys B Condens Matter 562:116
7. Peterson TA, Patel SJ, Geppert CC, Christie KD, Rath A, Pennachio D, Flatté ME, Voyles PM, Palmstrøm CJ, Crowell PA (2016). Phys Rev B 94:235309
8. Aadhityan A, Preferencial Kala C, John Thiruvadigal D (2018). Appl Surf Sci 449:799
9. Srivastava A, Olde Olthof LAB, Di Bernardo A, Komori S, Amado M, Palomares-Garcia C, Alidoust M, Halterman K, Blamire MG, Robinson JWA (2017). Phys Rev Appl 8:044008
10. Alidoust M, Halterman K, Valls OT (2015). Phys Rev B Phys Rev B 92:014508
11. Halterman K, Alidoust M (2016). Phys Rev B 94:064503
12. Alidoust M, Halterman K (2018). Phys Rev B 97:064517
13. Halterman K, Alidoust M (2018). Phys Rev B 98:134510
14. Mondal P, Bajpai U, Petrović MD, Plecháč P, Nikolić BK (2019). Phys Rev B 99:094431
15. Mahan GD (2016). J Electron Mater 45(3):1257
16. Lashgari H, Abolhassani MR, Boochani A, Sartipi E, Taghavi-Mendi R, Ghaderi A(2016) 90(8), 909
17. Kutepov AL, Kutepova SG (2003). Phys Rev B 67:132102
18. Ahuja R, Dubrovinsky L, Dubrovinskaia N, Osorio Gullen JM, Mattesini M, Johansson B, Le Bihan T (2004). Phys Rev B 69: 184102
19. Hao Y-J, Zhang L, Chen X-R, Li Y-H, He H-L (2008). J Phys Condens Matter 20:235230
20. Le Flem M (2008) J'er`ome Canel, St'ephane Urvoy. J Alloys Compd 465:269
21. Shin-Pon J, Wu T-Y, Liu S-H (2015). J Appl Phys 117:105103
22. Ramos AS, Nunes CA, Coelho GC (2006). Mater Charact 56:107
23. Shao X, Liu X, Zhang X, Wang J, Zhao M (2018). Phys Chem Chem Phys 20:3946
24. Sreenivasa Reddy PV, Kanchana V, Vaitheeswaran G, Ruban AV, Christensen NE (2017). J Phys Condens Matter 29:265801
25. Takamura Y, Nakane R, Sugahara S (2009). J Appl Phys 105: 07B109
26. Sreenivasa Reddy PV, Kanchana V (2014). AIP Conf Proc 1591: 1121
27. Premkumar M, Prasad KS, Singh AK (2009). Intermetallics 17:142
28. Sornadurai D, Sastry VS, Thomas Paul V, Flemming R, Jose F, Ramaseshan R, Dash S (2012). Intermetallics 24:89
29. Parsamehr S, Boochani A, Sartipi E, Amiri M, Solaymani S, Naderi S, Aminian A (2019) 40(7), 64
30. Kieven D, Klenk R (2010). Phys Rev B 81:075208
31. Hashemifar SJ, Kratzer P, Scheffler M (2005). Phys Rev Lett 94(9): 096402
32. Junfeng H et al (2019). Solid State Commun 299:113661
33. Frost W, Samiepour M, Hirohata A (2019). J Magn Magn Mater 484:100
34. Martens K et al (2015). Phys Rev Lett 115:196401
35. Alidoust M, Halterman K (2014). Phys Rev B 89:195111
36. Halterman K, Alidoust M (2016). Supercond Sci Technol 29: 055007

37. Alidoust M, Halterman K (2015). J Appl Phys 117:123906
38. Zhang R-w et al (2014). Solid State Commun 191:49
39. Griffin SM, Neaton JB (2017). Phys Rev Mater 1:044401
40. Cui B et al (2017). Phys Rev B 96:085134
41. Zheng F-b, Zhang C-w, Wang P-j, Li S-s (2013). J Appl Phys 113: 154302
42. Collins BA, Chu YS, He L, Haskel D, Tsui F (2015). Phys Rev B 92:224108
43. Hamaya K, Murakami T, Yamada S, Mibu K, Miyao M (2011). Phys Rev B 83:144411
44. Maeda Y, Narumi K, Sakai S, Terai Y, Miyao M (2011) 519(24) 8461
45. Han H, Feng T, Fan L, Zhao Z, Yao KL (2017). J Magn Magn Mater 438:95
46. Paudel R, Zhu J (2019). Vacuum 164:336
47. Slater JC (1964). Adv Quantum Chem 1:5564
48. Blaha P, Schwarz K, Madsen GKH, Kvasnicka D, Luitz J (2001) WIEN2K, an Augmented Plane Wave + Local Orbitals Program for Calculating Crystal Properties 3–9501031–1-2, Karlheinz Schwarz, Technische Universität, Wien, Austria
49. Perdew JP, Burke K, Ernzerhof M (1996). Phys Rev Lett 77:3865
50. Shi H, Ming W, Parker DS, Mao-Hua D, Singh DJ (2017) Prospective high thermoelectric performance of the heavily p-doped half-Heusler compound CoVSn. Phys Rev B 95:195207
51. Shatsalaa ME, Magetoa M, Manyalia G, Mghendi M (2016) Thermodynamic stability of ABX heavy elements of TaIrGe, TiIrSb, TaIrSn and ZrIrSb TCOs using the half-Heusler technique. Energy Procedia 93:191
52. Jamal M, Kamali Sarvestani N, Yazdani A, Reshak AH (2014) Mechanical and thermodynamical properties of hexagonal compounds at optimized lattice parameters from two-dimensional search of the equation of state. RSC Adv 4:57903
53. Mouhat F, Coudert FX (2014) Necessary and sufficient elastic stability conditions in various crystal systems. Phys Rev B 90:224104
54. Yildirim A, Koc H, Deligoz E (2012) First-principles study of the structural, elastic, electronic, optical, and vibrational properties of intermetallic Pd2Ga. Chin Phys B 21:037101
55. Brik MG (2010) First-principles calculations of electronic, optical and elastic properties of ZnAl2S4 and ZnGa2O4. J Phys Chem Solids 71:1435
56. Ahmadi S, Mehrabi M, Rezaei S (2019) Noushin Mardafkan. J Mol Struct 1191:165
57. Kaspar P, Sobola D, Dallaev R, Ramazanov S, Nebojsa A, Rezaee S, Grmela L (2019). Appl Surf Sci 493:673
58. Korpi AG et al (2019). Mater Res Exp 6(8):086463
59. Munira K, Romero J, Butler WH (2014). J Appl Phys 115:17B731

Publisher's Note Springer Nature remains neutral with regard to jurisdictional claims in published maps and institutional affiliations.